Numerical Study of the Motion of a Freely Falling Sphere in Fluid

Lei Liu[1,2], Haining Lu[1,2], Jianmin Yang[1,2], Tao Peng[1,2], Xinliang Tian[1,2]
[1]State Key Laboratory of Ocean Engineering, Shanghai Jiao Tong University
Shanghai, China
[2]Collaborative Innovation Center for Advanced Ship and Deep-Sea Exploration
Shanghai, China

ABSTRACT

Numerical study of the free-fall of a single sphere at different Reynolds numbers has been conducted with Computational Fluid Dynamics(CFD) method based on the engineering concerns of the dynamics of ore particles in vertical pipes in deep sea mining. A combination of Detached Eddy Simulation (DES) and the six-degree-of-freedom (6-DOF) motion solver was adopted. The sphere motion, the hydrodynamic forces on the sphere and the characteristics of the surrounding flow field were analyzed in detail. Different falling trajectories of the sphere were observed. The surrounding flow field gradually lost the symmetry with the increase of Reynolds number. The results of this article would provide a basic reference for the further investigation on motion of the multiple ore particles.

KEY WORDS: Free-fall; Reynolds number; sphere motion; flow field; hydrodynamic force.

INTRODUCTION

As the increasing demand of the natural sources in the world, deep sea deposits are considered as the most valuable alternative sources. Deep sea mining applications has been proposed since 1960s (Mero, 1965; Willums and Bradley, 1974; Chung, 1999; Chung, 2005; Chung, 2009). One of the most important issues in deep sea mining is the ore transportation from seafloor. Typically, ore particles can be transported vertically to the support vessels in the upward flow of water in a riser. Significant efforts have been dedicated to the vertical hydraulic transport system in deep sea mining (Engelmann, 1978; Bournaski et al., 2001; Xia et al., 2004; Chung et al., 2007; van Wijk, 2016).

Engelmann (1978) conducted experimental investigation on the hydrodynamic behaviors of ore particles in a vertical tube, and established the empirical equations for designing the hydraulic transport system in deep sea mining. Chung et al. (1998), Chung et al. (2001) and Chung et al. (2007) had a thorough investigation on the vertically upward transport in deep sea mining, including the transportation of spherical bead and non-spherical particles, the effects of particle shape and size, different particle behaviors over a wide range of Reynolds number in both Newtonian fluid and non-Newtonian fluids. Yoon et al. (1999), Yoon et al. (2001) and Yoon et al. (2008) studied the flow characteristics of the solid-liquid two-phase mixture in both vertical tubes and flexible hoses. Bournaski et al. (2001) and Xia et al. (2004) studied the hydraulic gradient caused by the fluid, the coarse particles and the collisions in the vertical pipes. Parenteau (2010) carried out numerical simulations to investigate the transient behaviors and pressure predictions for the risers by using Computational Fluid Dynamics (CFD) methods. Talmon and Rhee (2011) designed a close-loop system in the laboratory to conduct experiments on ore transport over large vertical distances. Sobota et al. (2013) experimentally investigated the velocities of ore particles and carrier liquid to determine the slip velocities for the artificial nodules in the vertical pipe. Vlasak et al. (2014) studied the influence of pipe inclination, solid concentration and mixture velocity on the characteristics of particle-water mixtures by using a pipe loop system. van Wijk (2016) carried out a study into flow assurance of the hydraulic transport system in deep sea mining and proposed a one-dimensional flow model to investigate the mechanisms leading to the riser blockage.

At the first stage of the research on vertical hydraulic transport, a comprehensive understanding of the motion of a single ore particle in Newtonian fluid may be the base of further study of the dynamics of multiple ore particles in pipe flow. In the present study, the ore particle was simplified as a sphere representing the very basic condition of particle motion in fluid. In the final state of vertical hydraulic transport, the drag force exerted on the particle is in balance with the gravitational and the buoyant forces; the particle always lags the fluid and the velocity difference between the particle and the fluid remains constant. Based on the theory of Galilean transformation, the particle motion in the upward flow is equivalent to the free-fall in still water in the steady state when ignoring the influence of the pipe wall. Therefore, the free-fall of a sphere in fluid is considered in our study.

The freely falling particles or objects in bounded and unbounded fluid have been widely investigated both experimentally and numerically since 1900s(Allen, 1900; Bromwich, 1929; Drazin, 1951; Preukschat, 1962; Christiansen and Barker, 1965; Ockendon, 1968; Stringham et al., 1969; Boillat and Graf, 1981). In recent years, Jenny et al. (2004) have studied the path instabilities of freely falling or ascending spheres in a Newtonian fluid using Direct Numerical Simulation (DNS) method.

Five different path regimes were identified, and a parametric space for path regimes of freely falling and rising spheres was summarized. And the results were experimentally validated by Veldhuis and Biesheuvel (2007). Yu et al. (2004) numerically investigated the sedimentation of a sphere and its radial migration in a Poiseuille flow in a vertical tube, and presented the flow features and the sphere motion at different Reynolds numbers. A comprehensive experimental study of freely falling and rising spheres was carried out by Horowitz and Williamson (2010) at different density ratios and Reynolds numbers. A new regime map of vortex wake modes was presented as a function of Reynolds number and density ratio Re-ρ_s/ρ_f. Moreover, Xiang et al. (2016a), Xiang et al. (2016b) and Xiang et al. (2017) conducted both theoretical and numerical investigation on the dropped objects in fluid. A new three-dimensional (3D) theory was proposed and a numerical tool was developed to predict the trajectory of the object underwater. Factors that affect the trajectories and the landing points were systematically studied.

Based on the open literature, the studies of the vertical transport of ore particles were mostly based on the experiments from which the flow field and the hydrodynamic forces were not easy to be measured. The numerical simulations using DNS method demand large amounts of computational resources, and a more efficient and reliable numerical method is still in need. In the present study, a combination of Detached Eddy Simulation (DES) and the six-degree-of-freedom (6-DOF) motion solver was adopted to have a detailed analysis of the free-fall of a sphere. The motion of the sphere, the surrounding flow field and the hydrodynamic forces have been investigated at different Reynolds numbers *Re*=184, 228, 285, 334 and 6400. Different falling trajectories, such as vertical, steady oblique, oscillating oblique, spiral and chaotic, were observed. With the increase of Re, the flow field varied from axial symmetry to plane symmetry, and finally became chaotic. The velocity distributions, the vortex structures of surrounding fluid field and the hydrodynamic forces on the particles were discussed to explain for different falling trajectories.

NUMERICAL METHOD

The CFD code STAR-CCM+ was adopted in our numerical simulations. The flow around the sphere was modelled with DES method, whereas the sphere motion was calculated by the 6-DOF motion solver. The results were all made dimensionless.

DES method

In this study, the flows arising around the sphere are turbulent at some Reynolds numbers, i.e. *Re* = 6400. Thus, either a turbulent model or the DNS method is required. Detached Eddy Simulation is a hybrid numerical method to model the turbulent which was first proposed by Spalart et al. (1997). It combines the features of Reynolds-Averaged Navier-Stokes (RANS) model in the boundary layer and Large Eddy Simulation (LES) in unsteady separate regions. When comparing to DNS method, DES method would save large amounts of computational resources and would be used in our work. The *k*-ω Shear Stress Transport (SST) model was adopted to simulate the near-wall fluid. Based on the work by Menter and Kuntz (2004), the dissipation term in the transport equation for turbulent kinetic energy has been modified with the coefficient ϕ:

$$\phi = max\left(\frac{l_t}{C_{des}\Delta}(1-F_2),1\right) \quad (1)$$

$$\phi = \begin{cases} 1 & if\ l_t < C_{des}\Delta \leftrightarrow RANS\ mode \\ > 1 & if\ l_t > C_{des}\Delta \leftrightarrow LES\ mode \end{cases} \quad (2)$$

where l_t is the calculated length scale of turbulent, Δ is the largest distance between the cell center under consideration and the cell centers of the neighboring cells, and F_2 is the blending function. The model constant C_{des} blends the values obtained from independent calibration of the *k*- ε and *k*-ω branches of the *k*-ω SST model, and is evaluated as follows:

$$C_{des} = C_{des,k-\omega}F_1 + C_{des,k-\varepsilon}(1-F_1) \quad (3)$$

where F_1 is the blending function.

6-DOF motion solver

The 6-DOF motion solver is used to simulate the free-fall of the sphere in response to the fluid-induced and the gravitational forces. The resultant force and moment exerted on the sphere are first calculated, and then used to solve the following governing equations of the motion:

$$m\frac{d\boldsymbol{V}}{dt} = \boldsymbol{f} \quad (4)$$

$$\boldsymbol{M}\frac{d\boldsymbol{\omega}}{dt} + \boldsymbol{\omega} \times \boldsymbol{M\omega} = \boldsymbol{n} \quad (5)$$

where m represents the mass of the body, $\boldsymbol{f}$ is the resultant force on the body, $\boldsymbol{V}$ is the velocity of the center of mass, $\boldsymbol{M}$ is the tensor of the moments of inertia, $\boldsymbol{\omega}$ is the angular velocity of the rigid body and $\boldsymbol{n}$ is the resultant moment on the body (CD-adapco, 2016).

The calculated results are all made dimensionless in the present study. The scales used to non-dimensionalize the results are: $L_0 = D$ for length, $T_0 = \sqrt{D/(\rho_s/\rho_f - 1)g}$ for time, $V_0 = \sqrt{(\rho_s/\rho_f - 1)gD}$ for velocity, $\omega_0 = \sqrt{(\rho_s/\rho_f - 1)g/D}$ for angular velocity, $F_0 = \rho_f g\pi D^3/6$ for force and $M_0 = \rho_f g\pi D^4/6$ for moment.

Computational domain and boundary conditions

The motion of a sphere with a diameter of *D* in a viscous fluid under the action of gravitational and hydrodynamic forces is considered. Fig 1 shows the computational domain and the boundary conditions. The boundary of the background region is set as velocity inlet with the value of zero, whereas the sphere surface is defined as no-slip wall.

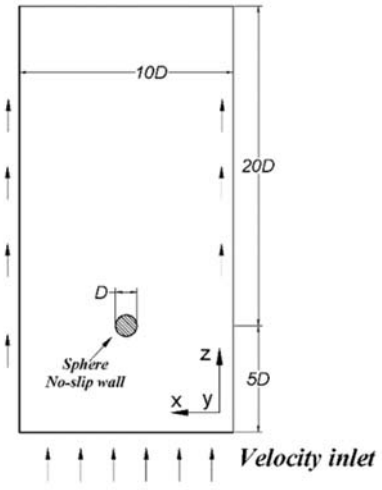

Fig. 1 Computational domain and boundary conditions

Overset mesh

Overset meshes are used to discretize the computational domain into a system of meshes with different features. As shown in Fig. 2, a cylindrical background region enclosing the entire computational domain and a smaller spherical overset region containing the moving sphere are generated. The spherical region is designed with a radius of $1.5D$ and moves with the sphere, and the 6-DOF motion solver is applied. An overset boundary is defined to separate the background region into active and inactive regions. The solutions on the two overlapping grids are implicitly coupled by means of interpolation through the cells attached to the overset boundary.

The computational domain is represented by sets of unstructured trimmed cells and prism layer cells, and the cutaway view of grid structures is illustrated in Fig.3. Additional refinements are applied in the zone containing the sphere and the vortex to capture details of the wake structures. The dimensionless height of the first layer of cells off the sphere surface is kept in the range of $y^+ < 1$ by the application of prism layer cells. The convective Courant number is always lower than 1 in most areas in the simulations.

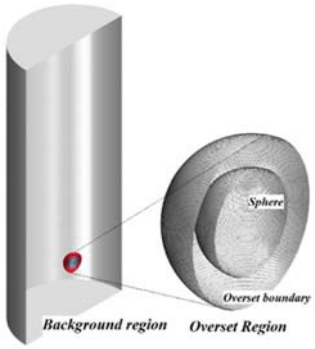

Fig.2 The overset mesh

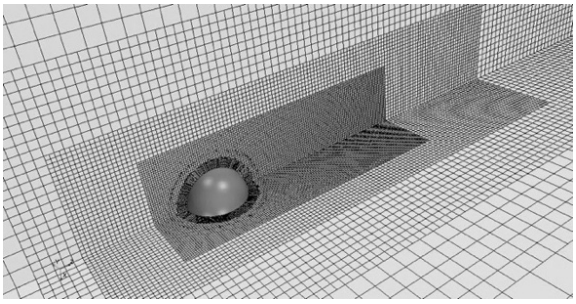

Fig. 3 Cutaway view of grid structures

Mesh and time-step validation

Spatial and temporal resolution tests have been conducted to prove the numerical solutions are mesh and time-step independent. Four different meshes and three different time-steps are selected. The calculated results, such as the vertical velocity of the sphere V_z, the frequency and amplitude of the periodic transverse motion f_{V_t} and A_{V_t}, and the drag coefficient C_d are compared at Re=285.

The results with different meshes are shown in Table 1. It is noted that the characteristics of the sphere motion in Cases A2, A3 and A4 reach a good agreement. The slight differences in Cases A3 and A4 indicate that the grid resolution in Case A3 is sufficient to solve the present problem. Table 2 shows the results with different time-steps. It can be inferred that the results are more sensitive to temporal resolution. As the time-step decreases from 1/50 to 1/100, the differences of the results significantly decrease, meaning that the non-dimensional time-step of 1/50 is sufficient to capture the sphere motion. Therefore, the grid with 960,153 cells and the time-step of $\Delta t/T_0 = 1/50$ are adopted for the simulations.

To further validate our numerical method, the results at different Reynolds numbers are compared with experimental (i.e. data of Mordant and Pinton (2000)) and numerical (i.e. DNS results of Rahmani and Wachs (2014)) results. The mean oblique angle α of the trajectory from the vertical axis at Re=240 is also included in Table 3. As shown in Table 3, the results in our simulation reach an acceptable agreement with the experimental and the DNS results at Re=41, 240, 600 and 4300. Thus, it is confident that the methods used in this study are reliable for simulating the free-fall of the sphere in viscous fluid.

Table 1. Spatial resolution tests at Re=285 ($\Delta t/T_0$=1/50)

Case	Cell Number	V_z	C_d	f_{V_t}	A_{V_t}
A1	430,780	1.4063	0.6742	0.0750	0.02700
A2	592,357	1.4024	0.6779	0.0738	0.02758
A3	960,153	1.4006	0.6797	0.0728	0.02772
A4	1,808,283	1.4001	0.6802	0.0722	0.02787

Table 2. Temporal resolution tests at Re=285 (cell number =960,153)

Case	$\Delta t/T_0$	V_z	C_d	f_{V_t}	A_{V_t}
B1	1/30	1.4048	0.6756	0.0713	0.02476
B2	1/50	1.4006	0.6797	0.0728	0.02772
B3	1/100	1.398	0.6822	0.073	0.02812

Table 3. Comparison of present results to experimental and DNS results

No.	Case	Re	α	V_z	C_d
1	Present study	41	-	0.877	1.734
2	Mordant and Pinton (2000)	41	-	0.847	1.858
3	Present study	240	4.63	1.361	0.720
4	Rahmani and Wachs (2014)	240	4.3	1.367	0.714
5	Present study	590	-	1.554	0.552
6	Mordant and Pinton (2000)	600	-	1.591	0.527
7	Present study	4336	-	1.835	0.396
8	Mordant and Pinton (2000)	4300	-	1.898	0.370

RESULTS AND DISCUSSIONS

Sphere motion

As shown in Fig. 4, different trajectories have been observed at different Reynolds numbers. The sphere falls vertically at Re=184. The vertical velocity is constant after T=30, whereas the transverse velocities are zero. The angular velocities are negligible. As the Reynolds number increases to Re=228, the trajectory is no longer vertical. The sphere finally falls in a steady oblique direction (approximately 5° from vertical axis, which is in agreement with Jenny et al. (2004) and Rahmani and Wachs (2014)) with constant vertical and transverse velocities. The angular velocities around the horizontal directions are steady, whereas that around the vertical axis is negligible. At Re=285, the sphere still falls in an oblique direction, however, with oscillations around it. Both the transverse and the vertical velocities oscillate around constant values with the frequency f=0.0728. It is worth noting that the sphere motion is within a constant plane in the final state. The angular velocities around the horizontal directions oscillate at the same frequency as that of the transverse velocities, whereas that around vertical axis is negligible. When the Reynolds

number increases to *Re*=334, the trajectory becomes spiral and the motion is no longer constrained within a single plane. The vertical velocity reaches a relatively stable oscillating state after T=100, whereas the onset of irregularity appears in the transverse velocities and the angular velocities around horizontal directions. In addition, the angular velocity around vertical axis is no longer zero. At *Re*=6400, the trajectory is fully chaotic, i.e. it is completely irregular over time, due to the entire turbulent flow around the sphere. The vertical velocity varies around a mean value, whereas the transverse velocities and the angular velocities are totally irregular.

Additionally, the drag coefficient can be calculated with $C_d = 4/(3V_z^2)$, where V_z is the non-dimensional vertical velocity of the sphere. Fig. 5 shows the drag coefficients of the sphere at different Reynolds numbers. It is clear that the calculated results agree well with the empirical formulas of drag coefficient of spherical particles summarized by Clift and Gauvin (1970) and Terfous et al. (2013).

In general, the trajectory of the sphere becomes more and more irregular with the increase of Reynolds number. When the flow around the sphere turns into turbulence, the sphere motion becomes totally chaotic.

Flow field

Typical counters of the vertical flow velocity and vortex structures (represented by λ_2-criterion proposed by Jeong and Hussain (1995)) at different Reynolds numbers are shown in Fig. 6. Clearly, the flow field is axisymmetric at *Re*=184. The vortex is constrained in a thin torus-shape region, and a complete recirculation region is formed after the sphere. As the Reynolds number increases to *Re*=228, the flow field becomes plane symmetric. The double-threaded vortex structures appear in the wake of the sphere. The threads are constant and slightly off-center, making the sphere fall in a steady oblique direction. At *Re*=285, the contour of the vertical velocity shows the flow around the sphere begins to sway. However, the flow field is still plane symmetrical. The vortex is shed periodically, which can be regarded as the pinch-off of the vortex structure, leading to the periodic transverse oscillations of the sphere. The symmetry of the flow field is broken at *Re*=334. The vortex shedding still exists, however, the vortex structures behind the sphere are twisted. The separation points of the vortex are not constrained in a constant plane, leading to the spiral trajectory of the sphere. At *Re*=6400, the flow field around the sphere is totally chaotic, resulting in the irregularity of the sphere motion.

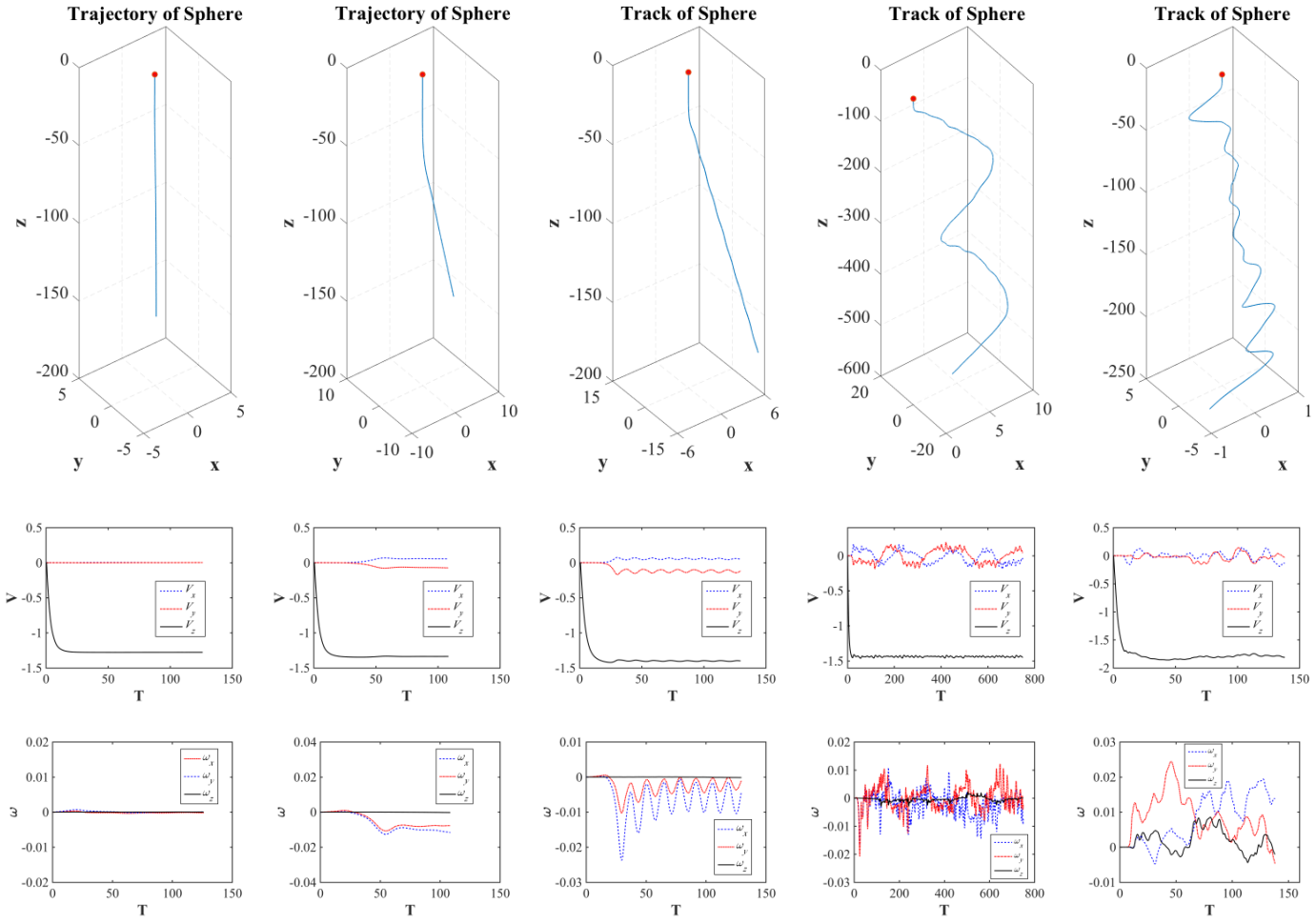

(a) Re=184 (b) Re=228 (c) Re=285 (d) Re=334 (e) Re=6400

Fig. 4 The trajectories, the velocities and the angular velocities of the freely falling sphere at *Re*=184, 228, 285, 334, 6400.

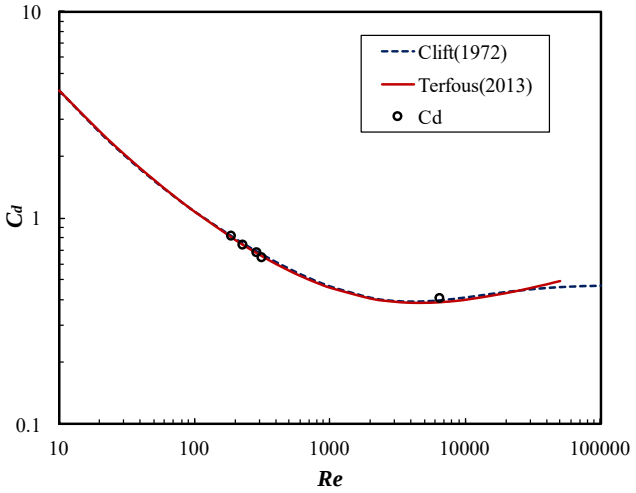

Fig. 5 The drag coefficients of the freely falling sphere

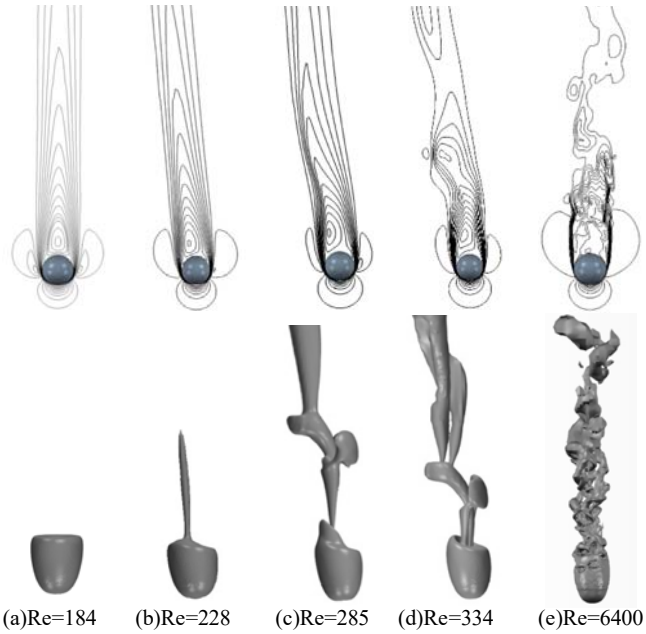

Fig. 6 The contours of vertical flow velocity and vortex structures at *Re*=184, 228, 285, 334 and 6400.

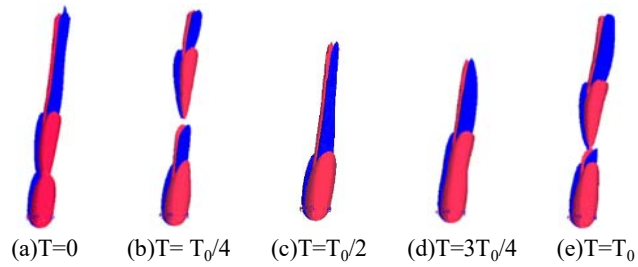

Fig. 7 Typical snapshots of the vortex structures within one oscillating cycle at *Re*=285.

Generally, the symmetry of the flow field is gradually broken with the increase of Reynolds number. The asymmetry of the flow field generates the horizontal hydrodynamic forces on the sphere, leading to the transverse motion of the sphere.

To gain better understanding of the flow field characteristics, typical snapshots of the vortex structures (represented by the iso-surface of the vertical component of the vorticity) within one oscillating cycle are shown in Fig. 7. Notably, the vorticity accumulates around the sphere and stretches behind the sphere over time. As the vorticity is generated continuously, the trailing component of the previous vorticity is shed, and such a process will be reproduced in the newly generated vorticity. The periodic vortex shedding would result in periodical lateral force and transverse oscillations of the sphere.

Hydrodynamic forces

The hydrodynamic forces, which are obtained by the integration of the pressure and shear stress on the sphere surfaces at different Reynolds numbers are presented in Fig. 8. Obviously, the vertical drag force F_z is constant after T=30, whereas the lateral forces and the moments are negligible during the freely falling process at *Re*=184. This explains for the vertical trajectory of the sphere. At *Re*=228, the lateral forces induce the transverse motion of the sphere once the sphere is released. After T=80, the lateral forces decay to zero and the sphere moves with a constant transverse velocity. The moments around the horizontal directions are nearly constant after T=80, leading to the constant angular velocities. The fluctuations of the hydrodynamic forces set in at *Re*=285, and induce the oscillations of the sphere motion. The frequencies of the hydrodynamic forces are coincident with those of the sphere velocities. As the Reynolds number increases to *Re*=334, the oscillations of the hydrodynamic forces become irregular. Both the frequency and the amplitude of the oscillations are no longer constant. Furthermore, the moment around the vertical axis is no longer zero, although the value is very small. At *Re*=6400, the hydrodynamic forces are totally chaotic. The vertical and lateral forces oscillate violently around their mean values. The oscillation of the moment around vertical axis is comparable to those around the horizontal directions, and is much larger than that in the lower Reynolds number conditions. Generally, as Reynolds number increases, the hydrodynamic forces gradually lose the regularities and eventually become chaotic.

Typically, the power density spectra of the lateral forces on the sphere at *Re*=334 and 6400 are presented in Fig. 9. It is noted that the lateral forces at *Re*=334 are dominated by two main frequencies (f_1=0.0575 and f_2=0.174). The lower frequency is smaller than the dominant frequency at Re=285 (f=0.0728), whereas the higher frequency is much larger. At *Re*=6400, the higher frequency at *Re*=334 disappears. The lateral forces are dominated by the low frequency f=0.053, which is only slightly shifted compared to the lower frequency at *Re*=334. In addition, a background noise can be seen in the already chaotic state.

CONCLUSIONS

Based on the engineering concerns of vertical hydraulic transport of ore particles in deep sea mining, numerical study of a freely falling sphere in fluid at different Reynolds numbers was conducted by using CFD method. A combined use of DES and 6-DOF motion solver has been adopted to provide an efficient and reliable simulation of the free-fall process. The sphere motion, the surrounding flow field and the hydrodynamic forces were analyzed in detail. As Reynolds number increases, five typical falling trajectories of the sphere: (1) vertical, (2) steady oblique, (3) oblique oscillating, (4) spiral and (5) chaotic, can be found. The surrounding flow field varies from axial symmetry to plane symmetry, and finally becomes chaotic. The hydrodynamic forces gradually lose the regularities and eventually become chaotic.

However, the sphere motion and the flow field were simulated without considering the effect of the pipe, and only a single falling sphere was investigated. Future research is planned to focus on the wall effect of the pipe and the dynamics of multiple spheres in the upward pipe flow.

ACKNOWLEDGEMENTS

The author would like to acknowledge the support of the National Key Research and Development Program of China (Project No. 2016YFC0304103).

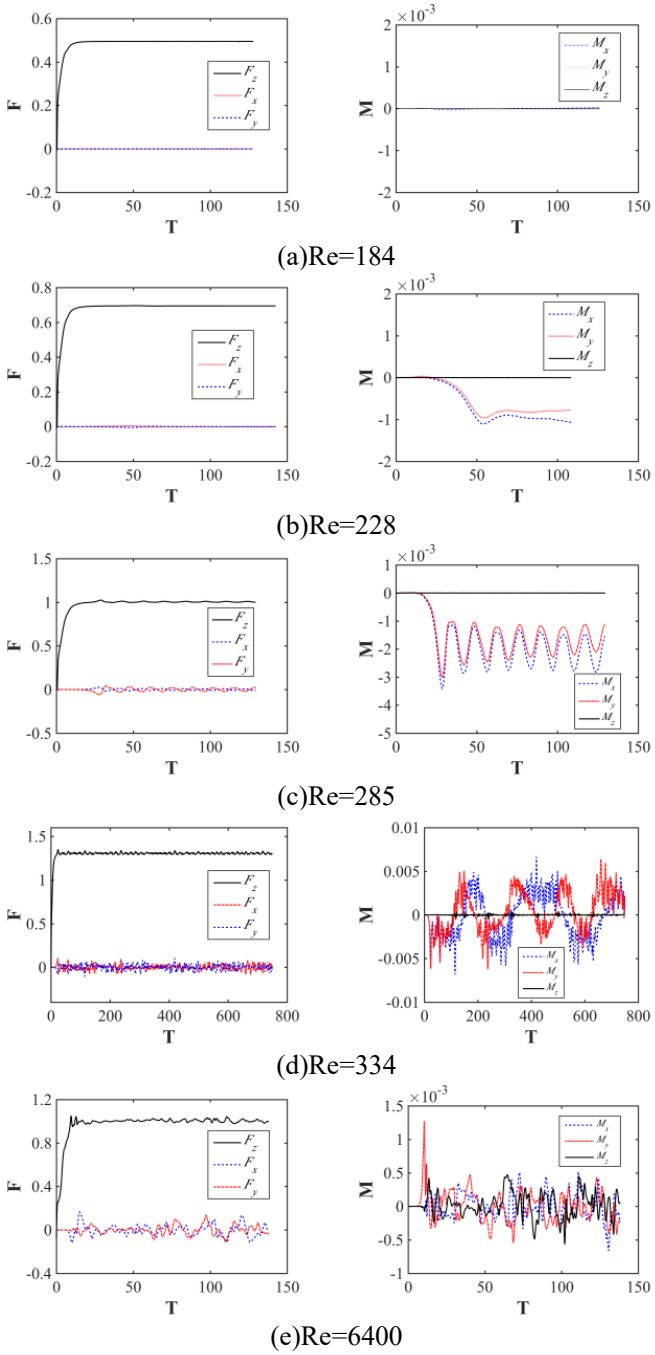

Fig. 8 Hydrodynamic forces on the sphere at *Re*=184, 228, 285, 334 and 6400.

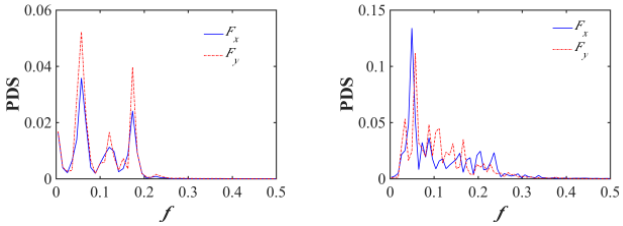

Fig. 9 Power density spectra of lateral forces on the sphere at *Re*= 334 and 6400.

REFERENCES

Allen, HS (1900). "XXXI. The motion of a sphere in a viscous fluid," *Philosophical Magazine Series 5*, 50(304), 323-338.

Boillat, JL, Graf, WH (1981). "Settling Velocity of Spherical Particles in Calm Water," *Journal of Hydraulic Engineering*, 107(10), 1123-1131.

Bournaski, E, Ivanov, I, Sobota, J, Berman, V (2001). "Hydraulic Losses Prognosis of Coarse Particles Flows in Vertical Pipes," *Proc 4th ISOPE Ocean Mining Symposium*, Szczecin, ISOPE, 139-143.

Bromwich, T (1929). "Motion of a sphere in a viscous fluid," *Mathematical Proceedings of the Cambridge Philosophical Society*, Cambridge Univ Press, 25, 369-383.

CD-adapco (2016). "User Guide, STAR-CCM+ Version 11.04," *CD-adapco*.

Christiansen, EB, Barker, DH (1965). "The effect of shape and density on the free settling of particles at high Reynolds numbers," *Aiche Journal*, 11(1), 145-151.

Chung, J, Yarim, G, Savasci, H (1998). "Shape effect of solids on pressure drop in a 2-phase vertically upward transport: Silica sands and spherical beads," *The 8th International Offshore and Polar Engineering Conference*, Montreal, ISOPE.

Chung, JS (1999). "Deep-Ocean Mining Issues and Ocean Mining Working Group (OMWG)," *Proc 3rd ISOPE Ocean Mining Symposium*, Goa, ISOPE.

Chung, JS (2005). "Deep-ocean Mining Technology: Development II," *Proc 6th ISOPE Ocean Mining Symposium*, Changsha, ISOPE, 1-6.

Chung, JS (2009). "Deep-ocean mining technology III: Developments," *Proc 8th ISOPE Ocean Mining Symposiumth*, Osaka, ISOPE.

Chung, JS, Lee, K, Tischler, A (2007). "Two-phase Vertically Upward Transport of Silica Sands In Dilute Polymer Solution: Drag Reduction And Effects of Sand Size And Concentration," *The 17th International Offshore and Polar Engineering Conference*, Lisbon, ISOPE.

Chung, JS, Lee, K, Tischler, A, Yarim, G (2001). "Effect of Particle Size And Concentration On Pressure Gradient In Two-Phase Vertically Upward Transport," *The 11th International Offshore and Polar Engineering Conference*, Szczecin, ISOPE.

Clift, R, Gauvin, WH (1970). "The motion of particles in turbulent gas streams," *Proceedings of Chemeca*, 1, 14–28

Drazin, M (1951). "The general motion of a sphere in a viscous liquid," *Mathematical Proceedings of the Cambridge Philosophical Society*, Cambridge Univ Press, 47, 142-145.

Engelmann, HE (1978). "Vertical Hydraulic Lifting Of Large-Size Particles-A Contribution To Marine Mining," *Proc 10th Offshore Technology Conference*, 732-735.

Horowitz, M, Williamson, CHK (2010). "The effect of Reynolds number on the dynamics and wakes of freely rising and falling spheres," *Journal of Fluid Mechanics*, 651, 251-294.

Jenny, M, Dušek, J, Bouchet, G (2004). "Instabilities and transition of a

sphere falling or ascending freely in a Newtonian fluid," *Journal of Fluid Mechanics*, 508, 201-239.

Jeong, J, Hussain, F (1995). "On the identification of a vortex," *Journal of fluid mechanics*, 285, 69-94.

Menter, F, Kuntz, M (2004). *Adaptation of eddy-viscosity turbulence models to unsteady separated flow behind vehicles*, The aerodynamics of heavy vehicles: trucks, buses, and trains. Springer, 339-352.

Mero, JL (1965). *The mineral resources of the sea*. Elsevier Oceanography Series, Amsterdam.

Mordant, N, Pinton, J-F (2000). "Velocity measurement of a settling sphere," *The European Physical Journal B-Condensed Matter and Complex Systems*, 18, 343–352.

Ockendon, J (1968). "The unsteady motion of a small sphere in a viscous liquid," *Journal of Fluid Mechanics*, 34(02), 229-239.

Parenteau, T (2010). "Flow Assurance for Deepwater Mining," *Proc 29th International Conference on Ocean, Offshore and Arctic Engineering*, Shanghai, American Society of Mechanical Engineers, 11-21.

Preukschat, AW (1962). *Measurements of drag coefficients for falling and rising spheres in free motion,* Ph.D., California Institute of Technology.

Rahmani, M, Wachs, A (2014). "Free falling and rising of spherical and angular particles," *Physics of Fluids*, 26(8), 083301.

Sobota, J, Vlasak, P, Petryka, L, Zych, M (2013). "Slip Velocities in Mixture Vertical Pipe Flow," *Proc 10th ISOPE Ocean Mining and Gas Hydrates Symposium*, Szczecin, ISOPE, 221-224.

Spalart, PR, Jou, WH, Strelets, M, Allmaras, SR (1997). "Comments on the Feasibility of LES for Wings, and on a Hybrid RANS/LES Approach," *Advances in DNS/LES*, Columbus, Greyden Press, 137–147.

Stringham, GE, Simons, D, B, Guy, H, P (1969). *The behavior of large particles falling in quiescent liquids*. US Government Printing Office.

Talmon, AM, Rhee, CV (2011). "Test Set-Up for Irregular Vertical Hydraulic Transport in Deep Ocean Mining," *Proc 30th International Conference on Ocean, Offshore and Arctic Engineering*, Rotterdam, American Society of Mechanical Engineers, 319-328.

Terfous, A, Hazzab, A, Ghenaim, A (2013). "Predicting the drag coefficient and settling velocity of spherical particles," *Powder Technology*, 239, 12-20.

van Wijk, JM (2016). *Vertical hydraulic transport for deep sea mining: A study into flow assurance.*

Veldhuis, CHJ, Biesheuvel, A (2007). "An experimental study of the regimes of motion of spheres falling or ascending freely in a Newtonian fluid," *International Journal of Multiphase Flow*, 33(10), 1074-1087.

Vlasak, P, Chara, Z, Konfrst, J, Krupicka, J (2014). "Effect of concentration and velocity on conveying of coarse grained mixtures in pipe," *Proc 24th International Ocean and Polar Engineering Conference*, Busan, ISOPE, 66-71.

Willums, JO, Bradley, A (1974). "MIT's deep sea mining project," *Proc 6th Offshore Technology Conference*, 1072-1076.

Xia, JX, Ni, JR, Mendoza, C (2004). "Hydraulic Lifting of Manganese Nodules Through a Riser," *Journal of Offshore Mechanics and Arctic Engineering*, 126(1), 72-77.

Xiang, G, Birk, L, Li, L, Yu, X, Luo, Y (2016a). "Risk free zone study for cylindrical objects dropped into water," *Ocean Systems Engineering*, Vol. 6, No. 4 (2016) 377-400.

Xiang, G, Birk, L, Yu, X, Li, X (2016b, in press). "Study on the Trajectory and Landing Points of Dropped Cylindrical Object with Different Longitudinal Center of Gravity," *International Journal of Offshore and Polar Engineering*, ISOPE.

Xiang, G, Birk, L, Yu, X, Lu, H (2017). "Numerical study on the trajectory of dropped cylindrical objects," *Ocean Engineering*, 130, 1-9.

Yoon, C-H, Kang, J-S, Park, Y-C, Kim, Y-J, Park, J-M, Kwon, S-K (2008). "Solid-liquid Flow Experiment With Real And Artificial Manganese Nodules In Flexible Hoses," *The 18th International Offshore and Polar Engineering Conference*, Vancouver, ISOPE.

Yoon, CH, Kim, IK, Kwon, KS, Kwon, SK, Kwon, OK, Kang, JS, Seo, CW (1999). "An Experimental Study On the Flow Characteristics of Solid-liquid Two-phase Mixture In a Vertical Tube," *The 9th International Offshore and Polar Engineering Conference*, Goa, ISOPE.

Yoon, CH, Kwon, KS, Kwon, SK, Lee, DK, Park, YC, Kwon, OK, Sung, WM (2001). "An Experimental Study On the Flow Characteristics of Solid-liquid Two-phase Mixture In a Flexible Hose," *The 11th International Offshore and Polar Engineering Conference*, Szczecin, ISOPE.

Yu, Z, Phan-Thien, N, Tanner, RI (2004). "Dynamic simulation of sphere motion in a vertical tube," *Journal of Fluid Mechanics*, 518, 61-93.